Development and experimental validation of a transient 2D numeric model for radiant walls

Joaquim Romaní[1], Luisa F. Cabeza[1], Alvaro de Gracia[2,*]

[1]GREA Innovació concurrent, INSPIRES Research Centre, University of Lleida, Pere de Cabrera s/n, 25001-Lleida, Spain

[2]Departament d'Enginyeria Mecanica, Universitat Rovira i Virgili, Av. Paisos Catalans 26, 43007-Tarragona, Spain

*Corresponding author: alvaro.degracia@urv.cat

Abstract

An experimental set-up consisting of a house like cubicle exposed to outdoor weather was used to validate a numerical model of a radiant wall. The 2D transient finite volume model used as inputs the indoor temperature, outdoor temperature, global solar radiation incident on a vertical surface, and temperature and flow of the supply water. The simulation results closely agreed with the temperature profiles and heat fluxes for the three studied orientations (East, South, and West). Furthermore, a parametric study was carried out with the radiant wall model, concluding that pipes spacing between 125 mm and 150 mm and depth between 45 mm and 65 mm minimized the temperature difference on the surface while maximizing the heat flux. Furthermore, a control strategy with shorter activation periods improved the heat transfer efficiency.

Keywords: Thermally Activated Building Systems (TABS); Radiant Walls; Radiant Heating; FVM; Numerical Simulation

Nomenclature

TABS	Thermally activated building systems		
GHE	Ground heat exchanger		

HVAC	Heating ventilation and air conditioning		
2D	Two-dimensional		
3D	Three-dimensional		
FEM	Finite elements model		
FVM	Finite volume model		
FDM	Finite difference model		

σ	Stefan-Boltzmann constant ($W \cdot m^{-2} \cdot K^{-4}$)	Subindex	
K	Conductivity ($W \cdot m^{-1} \cdot K^{-1}$)	in	Indoor
Cp	Specific heat ($kJ \cdot kg^{-1} \cdot K^{-1}$)	out	Outdoor
P	Density ($kg \cdot m^{-3}$)	w	Water
Ɛ	Emissivity	brick	Alveolar brick
A	Solar absorptivity	insu	Insulation
H	Convection heat transfer coefficient ($W \cdot m^{-2} \cdot K^{-1}$)	fibr	Fibrocement board
T	Temperature (ºC)	Rad	Radiation ($W \cdot m^{-2}$)
t	Time (s)	rad_s	Solar radiation
V	Volume (m^3)	rad_th	Thermal radiation
J	Radiosity ($W \cdot m^{-2}$)	sky	
G	Irradiosity ($W \cdot m^{-2}$)	s_incident	Measured incident radiation
Q	Heat flux ($W \cdot m^{-2}$)		

1 Introduction

Reports of the International Energy Agency (IEA) show that buildings represent about 32 % of global energy use and 10 % of direct CO_2 emissions, and in case district heating and electricity

production is taken into account, the energy related CO_2 emissions associated to buildings could rise up to 30 % [1]. In that context, thermally activated building systems (TABS) were identified as a promising technology to tackle on the reduction of energy use in buildings. Consequently, much research was conducted on TABS as presented on Rhee and Kin historical review [2], Xu et al. review on pipe-embedded structures [3], Xu et al. review on hollow core slabs [4], Romaní et al. review on control and simulation of TABS [5] and Rhee et al. review on key issues for radiant heating and cooling [6].

Consisting of pipes embedded in the building structure, TABS main advantages are the heat exchange by radiation, the use of building big surfaces, and the high thermal inertia. On one side, heat exchange by radiation can improve comfort by a better control of the mean radiant temperature [7], and therefore better management of operative temperature. Moreover, control of operative temperature range through mean radiant temperature allows a wider indoor air temperature range, which can reduce ventilation loses [8]. However, TABS energy efficiency is based on availability of large surfaces, which allow for a significant heat flux even at low temperature gradient between the heating or cooling fluid and the indoor space [9]. This feature enables low temperature heating and high temperature cooling, which increases the potential for renewable energy use for cooling [10,11] and heating [12,13]. Other advantages of TABS are the quiet operation, the low draught risk, and their integration to building design.

The main drawbacks of TABS are related to their complex control, which also involves the coordination with a ventilation system to deal with latent heat loads. Additionally, there are also acoustic issues and a higher investment cost than conventional HVAC [6]. Furthermore, the assets of TABS imply intrinsic difficulties on their design and operation. On one side, TABS imply the use of thermal mass and thermal lag, and only transient calculations can correctly represent the performance of these systems. Moreover, TABS heat exchange by radiation and direct interaction with the building structure add complexity to calculations. In order to overcome the design and control issues, simulation models were developed. These were used for optimizing TABS design and for simulating their interaction with the building, the supply system, and the controllers.

On this subject, Zmeureanu and Fazio [14] developed a transient 2D finite difference model (FDM) for hollow core concrete ventilated slabs. This model was coupled to a building model to study the reduction of the cooling load by ventilation of the hollow core slabs with night air. Antonopoulos and Democritou [15] also used 2D FDM to model roof slabs under periodic steady state conditions. In this case the objective was to study the design parameters that most affect to the TABS performance. Following this research, Antonopoulos and Tzivandis [16]

developed a transient 3D FDM model that allowed calculating the indoor temperature, the temperature distribution, and the fluid temperature variation along the pipe. Also finite elements models (FEM) were applied to TABS, as on Krzaczek and Kowalzuk [17] study of a thermal barrier (TB) with a 3D model. There the objective was to study the reduction of the cooling loads by keeping the active layer of the wall (layer containing the embedded pipes) at a constant temperature. Alternatively, Jin et al. [18] developed a 2D finite volume model (FVM) with a composite grid. A rectangular grid was applied as a base mesh for the slab, but the pipes were discretized with a polar grid. This hybrid mesh was used in a parametric study to analyse the influence of the pipes thickness, among other parameters. Finally, Shin et al. [19] developed design charts that show the relationship between heat flux and surface temperatures. The distribution of surface temperatures was obtained with the TRISCO simulation tool, which uses 3D steady state finite difference method. However, as the software worked with an orthogonal mesh the embedded pipes were transformed to virtual square pipes with equivalent inner surface.

Numerical modelling is an important tool to study TABS design and performance. However, it has some drawbacks. First, detailed simulation of all characteristics of an actual system is very complex and time consuming. Furthermore, many specific parameters can be unknown and uncertain. Consequently, modelling of TABS requires assumptions and simplifications. Usual assumptions are uniform and isotropic properties of materials and constant or correlated heat transfer coefficients, among others. Furthermore, considering symmetry or specific boundary conditions can simplify a model to 2D or 1D. All assumptions and simplifications introduce error to the model, therefore, the accuracy has to be validated, preferably with experimental data. On the other side, numerical modelling usually requires a high computational effort because of iterative processes. As a result, reduction of computational time is one of the main issues for numerical simulation of TABS, especially if coupling with building simulation environments is required. As an example, Holopainen et al. [20] attempted to reduce the computational effort by using uneven gridding with node distance increasing in geometric series, which reduced the size of the mesh without losing accuracy. Increasing the details and physics of a model can increase its accuracy; however, this will usually increase the computational effort. Consequently, numerical modelling requires a balance between detail and simulation time. It is here where model validation is especially useful, as it helps to ensure that the assumptions made to reduce the computational effort are reasonable and do not deviate the numerical results from the real performance of the system.

Despite the importance of validation in modeling and simulation of vertical TABS, literature of validated models in this area is recent. Instead of this, models were verified with other models

or analytical solutions. On this topic, finite difference model in frequency domain of a pipe-embedded envelope was developed and verified with a computational fluid dynamic model (CFD) model [21], this was later used for verification of simplified semi-dynamic lumped model [22]. Finally, those two models were validated with a laboratory experimental set-up consisting in a controlled temperature room separated in two spaces by a pipe-embedded wall [23,24]. Furthermore, a 3D CFD model developed in fluent of a pipe-embedded wall [25] was validated using data of a previous experiment on ceiling embedded piping [26]. Finally, a neural network model of a radiant wall was validated with an experimental set-up consisting in a room under laboratory controlled conditions [27]. However, simulation studies of vertical TABS without validation are still presented. Furthermore, the validation research found in the literature obtained the data from laboratory controlled test, no examples were found were data from actual outdoor conditions was used. This is relevant, as phenomena such as wind, rain, and dirt among other add complexity to boundary conditions, and thus more assumptions are required.

This paper presents the development and validation of a numerical model for a radiant wall. The data for the validation was obtained from an experimental set-up consisting in a house-like cubicle. This set-up was under real outdoor conditions and allowed to study the performance of radiant walls in different orientations. Furthermore, the house-like cubicle allowed studying the behaviour of the radiant walls in actual operation conditions of a building, but controlling and limiting the complex interaction of all the parameters existing in a real building.

Finally, the validated model was used in a parametric study to appropriately select design and control parameters of the radiant wall. Considering the wall design is limited by structure constraints the main variables for the design of a radiant wall are the spacing and depth of pipes. The study was focused on the influence of these parameters on indoor surface temperature differences and heat flux provided by the pipes. Furthermore, the influence of the intermittent heating supply on the total heat supplied was studied in terms of the length of heating period.

2 Experimental set-up

The experimental set-up shown in Figure 1 consisted in a house-like cubicle installed in an experimental test-site (Puigverd de Lleida, Spain). The cubicle was built with 285x185x195 mm alveolar bricks which had 16 mm diameter polyethylene pipes embedded 36 mm depth from the inner surface in grooves spaced 150 mm. On the outdoor skin the wall was insulated with 60 mm of expanded polystyrene protected from the outdoor by 5 mm fibrocement boards. The

schematic composition of the radiant wall is shown in Figure 2 and the physical properties of the materials are summarized in Table 1.

The radiant walls of the cubicle were distributed in five loops connected to a common manifold. East, West, and North walls had one loop each, while South wall had two loops. The north wall only had one loop because of the presence of two doors, as shown in Figure 3. Each loop was designed to have the same pipe length so that pressure loses and flow were the same. Furthermore, the flow and return pipes in each loop were placed alternatively as shown in Figure 3 so that temperature in the wall was uniform.

The heat was supplied by an EcoGeo B2 geothermal heat pump [28]. On the evaporator side, the heat pump was connected to two boreholes, each having two U-pipes of 20 m and 40 m deep. On the condenser side, the hot water was supplied to the radiant wall loops through a manifold, this had flow regulator valves that ensured equal flow rate at each loop.

More details about the experimental set-up are presented in previous studies [11,12].

Figure 1. Cubicle used for experimental validation

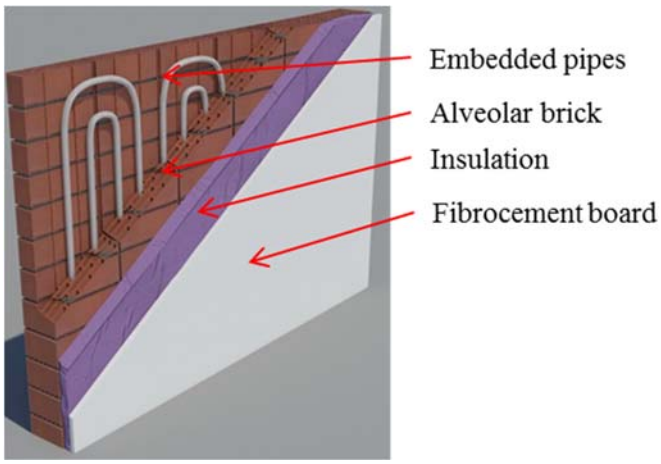

Figure 2. Radiant wall scheme

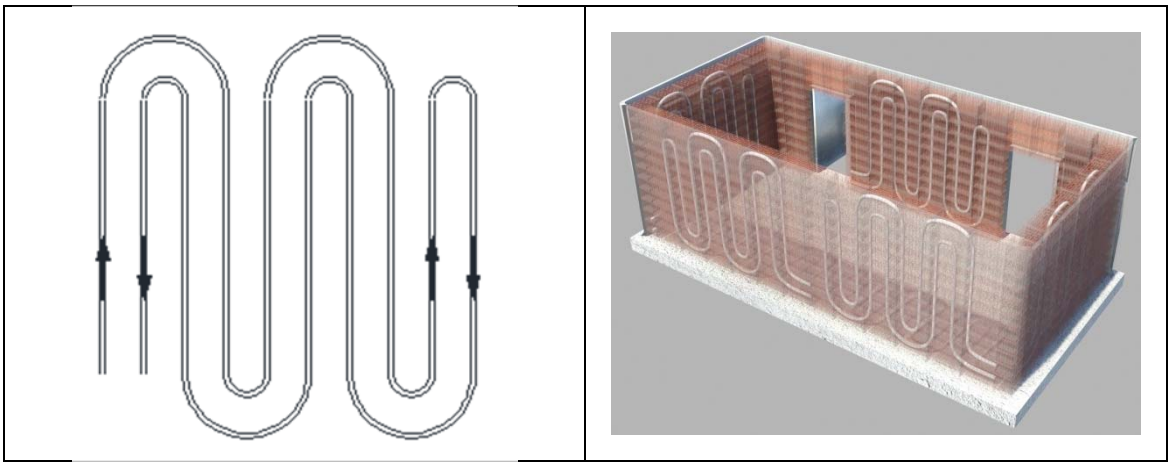

Figure 3. Radiant wall loops scheme (left) and distribution of the loops in the cubicle (right)

Table 1. Materials physical properties

	Brick	Insulation	External layer
Material	Alveolar brick	Expanded polystyrene	Fibrocement board
Density ($kg \cdot m^{-3}$)	1 000	35	1 600
Specific heat ($J \cdot kg^{-1} \cdot K^{-1}$)	880	1 130	840
Conductivity ($W \cdot m^{-1} \cdot K^{-1}$)	0.58	0.032	0.75
Emissivity (thermal)	0.8	-	0.6
Absorptivity (solar)	-	-	0.9
Width (mm)	185	60	5

3 Numerical model description

3.1 Model description and assumptions

The radiant wall was simulated with a transient two-dimensional finite volume model (FVM), the governing equation was as follows:

$$k \cdot \frac{\partial^2 T}{\partial x^2} + k \cdot \frac{\partial^2 T}{\partial y^2} = \rho \cdot c_p \cdot \frac{\partial T}{\partial t}$$

(Eq. 1)

On the measured data the maximum temperature gradient between pipe inlet and outlet was 5 K which was about 0.12 $K \cdot m^{-1}$. In these conditions, a reasonable assumption was to consider that

the fluid temperature remained constant along the pipe at the average measured fluid temperature. First, this allowed applying symmetry between pipes, and then the control volume was delimited by two adiabatic surfaces, one at half distance between pipes and the other cutting through the pipe centre. Second, the constant fluid temperature allowed applying 2D conditions as there was no heat flux in the pipe direction. For validation purposes, the temperature of the fluid was considered as the average between the inlet and outlet temperature measured experimentally.

In order to simplify the discretization, the pipe was assimilated as square duct with the same surface area [19]. As the pipe diameter was small compared to the bulk size of the wall and the heat transfer was mainly influenced by the low thermal conductivity of the brick the assumption was applicable. Furthermore, the thermal resistance of the pipes was disregarded.

Thermo-physical properties of solids were considered as homogeneous, isotropic and constant. Furthermore, the contact thermal resistance between solids was not considered. For radiation calculation the surfaces were considered as grey-diffuse. On the other side, thermo-physical properties of water were considered as a function of temperature.

3.2 Meshing and boundary conditions

The control volume was discretized with an orthogonal mesh of finite volumes as shown in Figure 4.

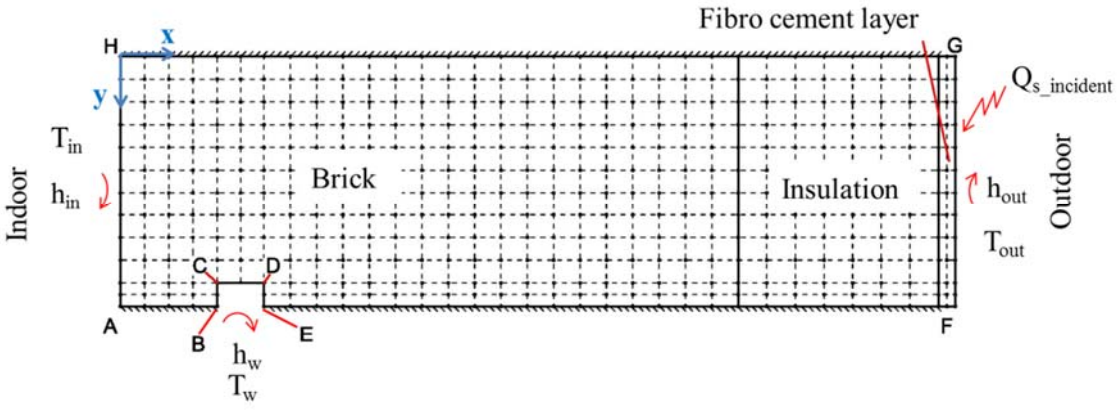

Figure 4. FVM discretization for the radiant wall (x axis normal to the wall surface, y axis parallel to the floor surface)

The boundary conditions were:

$\frac{\partial T}{\partial y} = 0$ on surfaces AB, EF, and GH

(Eq. 2)

$k_{brick} \frac{\partial T}{\partial x} = h_{in} \cdot (T_{in} - T)$ on surface AH

(Eq. 3)

$k_{brick} \frac{\partial T}{\partial x} = h_w \cdot (T - T_w)$ on surfaces BC

(Eq. 4)

$k_{brick} \frac{\partial T}{\partial y} = h_w \cdot (T - T_w)$ on surfaces CD

(Eq. 5)

$k_{brick} \frac{\partial T}{\partial x} = h_w \cdot (T_w - T)$ on surfaces DE

(Eq. 6)

$k_{fibr} \frac{\partial T}{\partial x} = h_{out} \cdot (T - T_{out}) - Q_{rad\_s} + Q_{rad\_th}$ on surface FG

(Eq. 7)

As previously said, the control volume was simplified with symmetry assumptions. This was represented with surfaces AB, EF, and GH in Figure 4 being adiabatic, and then Eq. 2 was applied.

On the indoor surface (AH), the heat transfer coefficient in Eq. 3 (h_{int}) was considered with a combined radiation and convention heat transfer coefficient obtained according to UNE-EN ISO 6946 [29], which combines convection and radiation. Furthermore, the heat transfer in the pipes, surface BC-CD-DE, was applied only when there was flow. In case the fluid was not circulating, the heat transfer coefficient in Eq. 4 to Eq. 6 (h_w) was considered as "0". In the opposite case, when flow was present, the heat transfer coefficient (h_w) was calculated with Chilton-Colburn correlation [30]. Due to the length of the pipes, the flow was considered developed in all cases. Moreover, the heat transfer coefficient was calculated considering the actual circular pipe, which was equivalent in surface to the rectangular pipe of the meshing. Moreover, the roughness of the polyethylene pipes was very low ($3 \cdot 10^{-6}$ m) which resulted in a

relative roughness around 0.0002. According to Moody diagram, for Re below 10^5 the friction factor with the above relative roughness is equal to and smooth surface.

On the external surface, corresponding to surface FG, the convective heat exchange in Eq. 7 (h_{ext}) was considered with a constant value obtained from UNE-EN ISO 6946 [29]. In addition, radiation heat transfer between the facade and the outdoor ambient was calculated with the radiosity and irradiosity method. The calculation for solar radiation was simplified considering only the solar absorptivity of the surface and the incident solar radiation, as shown in Eq. 8. On the other side, thermal radiation was calculated considering the sky as a blackbody with a T_{sky} according to Eq. 9 [31]. Then, radiosity and irradiosity method was applied considering a sky emissivity of "1" and a view factor of "1" between the facade and the sky, which resulted in Eq. 10 to Eq. 13.

$$Q_{rad\_s} = A_{s\_fibr} \cdot Q_{s\_incident}$$

(Eq. 8)

$$T_{sky} = 0.0552 \cdot T_{out}^{1.5}$$

(Eq. 9)

$$J_{fibr} = \varepsilon_{fibr} \cdot \sigma \cdot T_{fibr}^4 + (1 - \varepsilon_{fibr}) \cdot G_{fibr}$$

(Eq. 10)

$$G_{fibr} = J_{sky}$$

(Eq. 11)

$$J_{sky} = \sigma \cdot T_{sky}^4$$

(Eq. 12)

$$Q_{rad\_th} = J_{fibr} - G_{fibr}$$

(Eq. 13)

Finally, the thermal radiation on was obtained by solving Eq. 13 with Eq. 9 to Eq. 12, resulting in Eq.14.

$$Q_{rad\_th} = \varepsilon_{fibr} \cdot \sigma \cdot T_{fibr}^4 - \varepsilon_{fibr} \cdot \sigma \cdot 9.28445 \cdot 10^{-6} \cdot T_{out}^6$$

(Eq. 14)

3.3 Validation data

The data for the model validation was obtained from a test carried out from October 15th to 16th, 2016, both included. However, the temperature map of the wall was initialized with data from the previous three days. During this test the heat pump followed a pseudo-random binary series activation schedule with a set-point of 30 ºC. This operation avoided cyclic activation, which should help to validate that the model describes accurately the radiant wall behaviour in different conditions. The boundary conditions for the validation period are shown in Figure 5, note that water temperature in the graph is already average temperature between inlet and outlet.

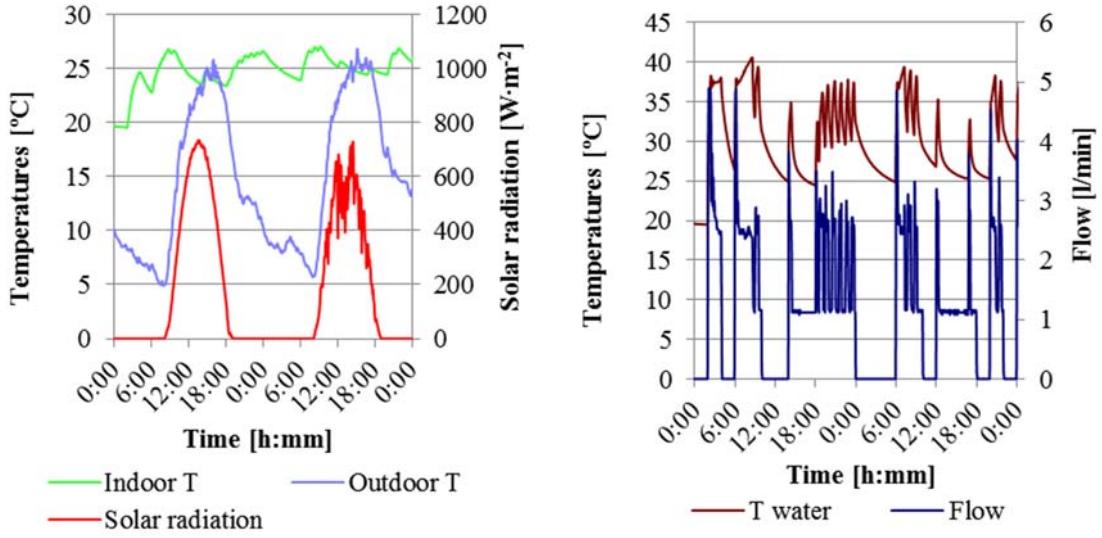

Figure 5. Boundary conditions for validation test

The reference values were obtained from two temperature sensors in the East, South and West walls. The location of the sensors was equivalent to position H in Figure 4 for the indoor surface and to position G in Figure 4 for outdoor surface. Additionally, the heat flux supplied to the radiant wall through the embedded pipes was compared. As the model was 2D, the heat flux obtained in the simulation was multiplied by the length of the pipe in each loop.

3.4 Parametric study methodology

The parametric study consisted of two parts. In the first, the design of the radiant wall was studied through two of its main parameters, the depth and spacing of the pipes. Second, the effect of an intermittent operation of the heat transfer efficiency was analysed.

The design of a wall in the envelope may be constrained by local building codes. These usually define the width and minimum stead-state transmittance (U-value) of the wall. Consequently, the main parameters for the design of the radiant walls are related to the spacing and depth of the pipes. The parametric study analysed the influence of these two variables on the maximum indoor surface temperature difference and on the heat flux on pipes surface and indoor surface. Furthermore, the maximum indoor temperature difference was measured as the instantaneous maximum gradient along the simulated period.

Regarding the influence of the intermittent operation, the control strategy consisted of consecutive active and inactive periods of the same time length, as shown in Figure 6. Six different strategies were implemented, with supply periods of 0.5 h, 1 h, 2 h, 4 h, 6 h, and 12 h. The total amount of hours per day with heating supply was the same in each strategy, 12 h.

The boundary conditions of the parametric study were constant indoor temperature of 21 ºC and the same outdoor conditions of the validation experiment (Figure 5). Furthermore, water supply was fixed at a flow of 2.5 l/min at average temperature of 30 ºC. Heating supply followed the strategies described above

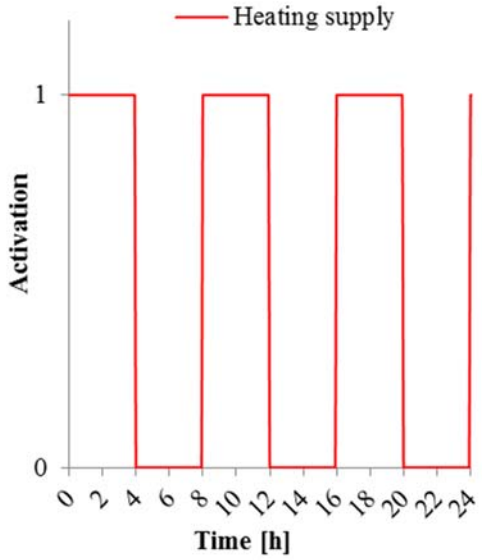

Figure 6. Heating supply control strategy (example for 4 h activation control strategy)

4 Validation results

The validation test showed good agreement between measured and simulated values as shown in Figure 7. The model followed the temperature variations on the points corresponding to the sensors positions, achieving the same behaviour with small error in the three orientations. As summarized in Table 2 the average temperature error on indoor surface was kept below 2% in all walls, while outdoor surface temperature had a maximum average error of 13% on the West wall. Moreover, the total heat flux in each wall had and error below 2.4 %. Consequently, the model was representative of the radiant wall and it was able to predict its behaviour with the input data of indoor temperature, outdoor temperature, vertical solar radiation, supply water flow, and supply water average temperature.

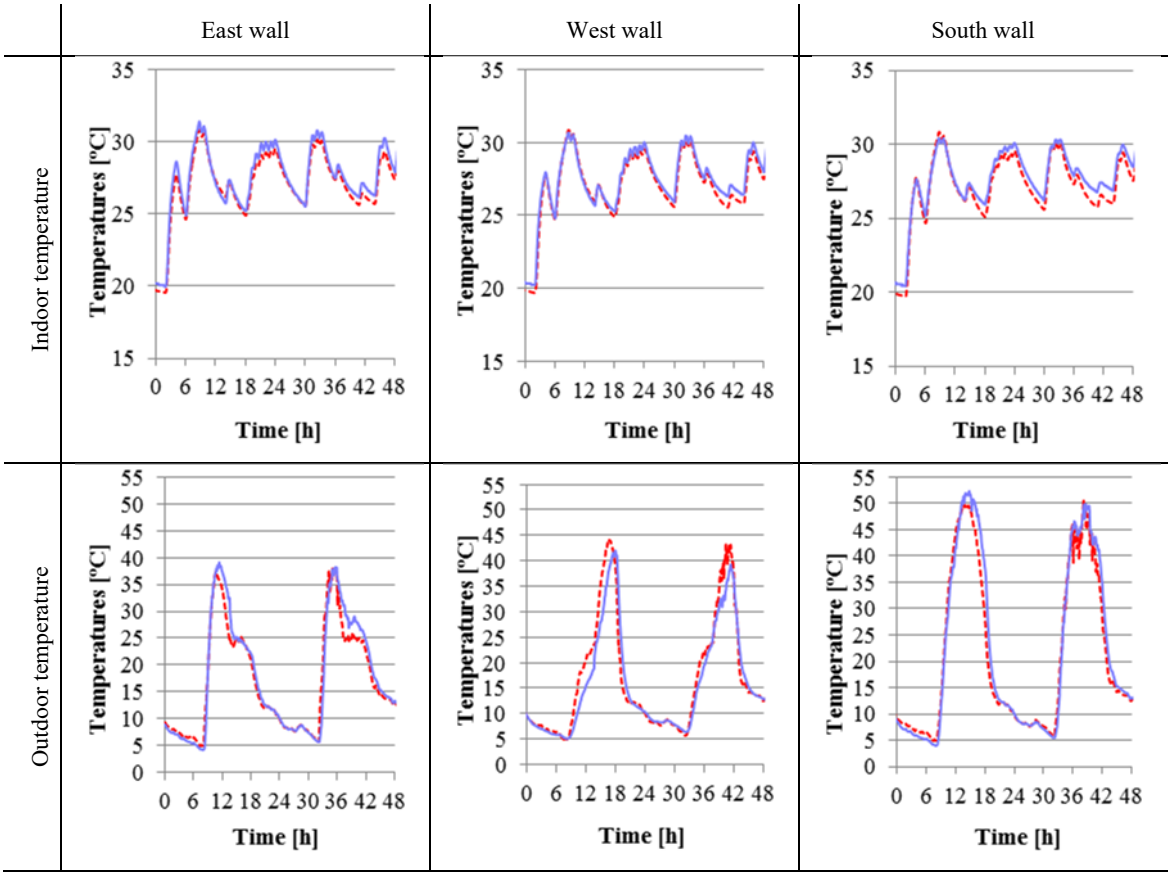

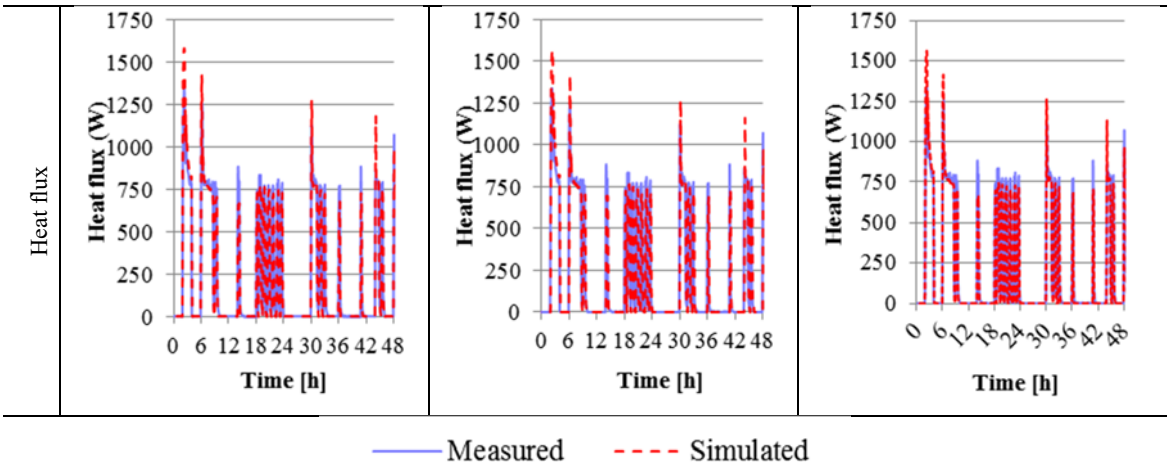

Figure 7. Comparison between experimental data and simulation results of heat flux, and outdoor and indoor temperature of the radiant wall

Table 2. Simulation error results

	Indoor surface temperature average error	Outdoor surface temperature average error	Heat flux error
East	1.7 %	7.9 %	0.12 %
West	1.4 %	12.8 %	0.95 %
South	1.9 %	8.2 %	2.39 %

The good agreement between simulated and measured heat flux indicated that 2D assumption was reasonable. Furthermore, the influence of the supply temperature was analysed in Figure 8, in which the heat delivered was calculated in a temperature range between the measured inlet and outlet temperature of the fluid. The results showed that the delivered heat had a symmetric pattern around average temperature, with an error of 15 % if the fluid was considered constant at inlet temperature and -15 % if it was considered at outlet temperature. Despite the thermal properties of water are non-linear with temperature, the temperature gradient in the radiant wall was low enough to result in small variations in thermal properties. Consequently, assuming no temperature variation in the pipes direction by considering constant fluid temperature at the average between inlet and outlet was acceptable.

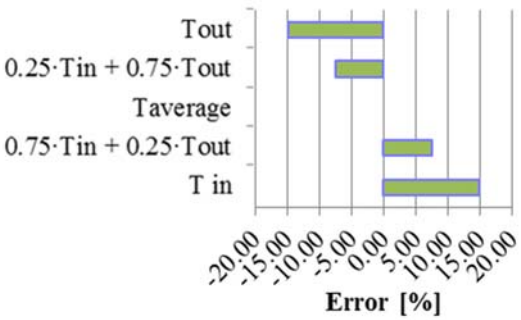

Figure 8. Indoor surface heat error dependent off assumed fluid temperature (referenced to average temperature)

5 Parametric study results

The parametric study was carried out for the different control strategies, however, as the results were equivalent for each strategy the effect of spacing and depth of pipes is shown for the 4 h control strategy. On the other side, the effect of the control strategy is presented for the values of the depth and spacing of the actual radiant wall (150 mm spacing and 36 mm depth).

5.1 Influence of depth and spacing

The influence of pipe depth and spacing into indoor temperature gradient is shown in Figure 9. Both parameters had high impact on the temperature gradient at their low values, but as both spacing and depth increased the temperature gradient stabilized.

At low spacing the heat waves from each pipe superposed resulting in a more uniform temperature field in the pipes plane. However, as the spacing increased there was more mass to be heated by each pipe, this together with the low conductivity of the brick resulted in a significant temperature gradient between pipes, which was also reflected in the indoor surface temperature.

Similarly, when the pipes were embedded at low depth, the heat wave reached the indoor surface faster on the nearest point to the pipe, resulting in a high temperature gradient in the surface. This gradient drastically dropped at increasing the depth at low values, however, at higher depth values the temperature gradient also increased again, although slowly. However, between depth between 45 mm and 65 mm the temperature gradient was minimized at the studied spacing range.

The study of the effect of the depth and spacing to indoor surface temperature difference suggested that this value was minimized for depth values between 45 mm and 65 mm and spacing values below 150 mm. However, lower spacing implies more meters of piping per square meter of wall, this would result in higher pressure losses, and thus higher energy use of the circulation pumps.

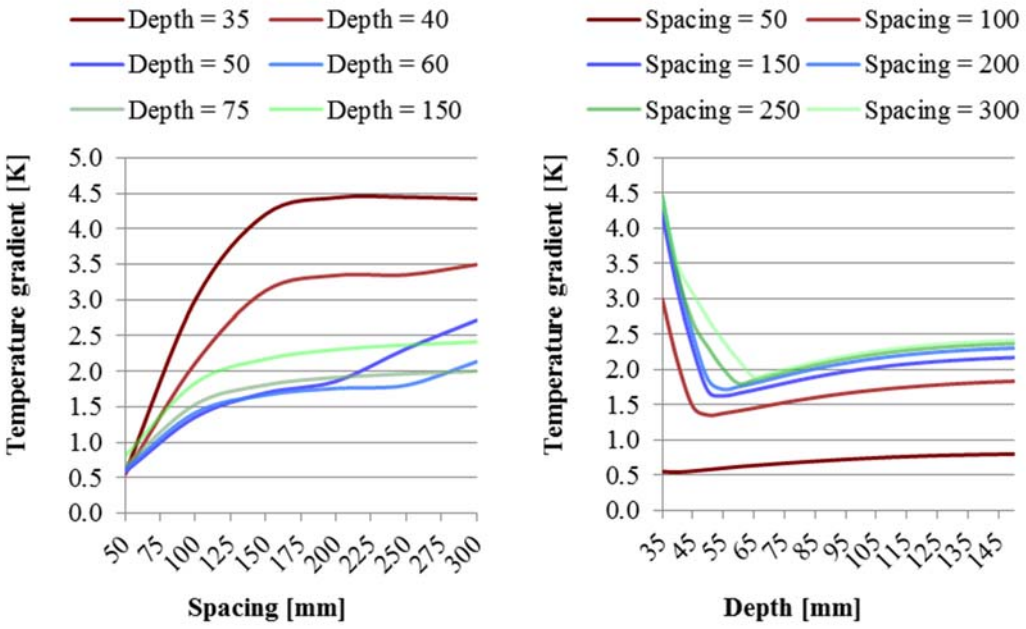

Figure 9. Influence of depth and spacing to maximum temperature difference on indoor surface

As shown in Figure 10 the heat flux supplied by the pipes per radiant wall surface decreased with the spacing. Higher spacing resulted in less pipes per square meter of wall, therefore, less heat exchange surface in the pipes per wall surface, which resulted in less heat transfer.

Additionally, the heat flux supplied by the pipes decreased with depth, as shown in Figure 10. As depth values increased, the pipes were nearer to insulation and further from the indoor surface. This implied that more mass of the wall had to be heated before the heat could be released to the indoor space. This together with the low conductivity of the brick caused the brick to accumulate more heat and increase its temperature. As a result, the heat flux was reduced by the lower temperature gradient between the supply water and the wall temperature.

Regarding the heat flux provided by the radiant wall, both the depth and the spacing should be minimized. However, low spacing implies longer piping per wall surface, which results in higher pressure losses. Consequently, the selection of spacing must balance the heat transfer aspects as well as the hydraulics parameters.

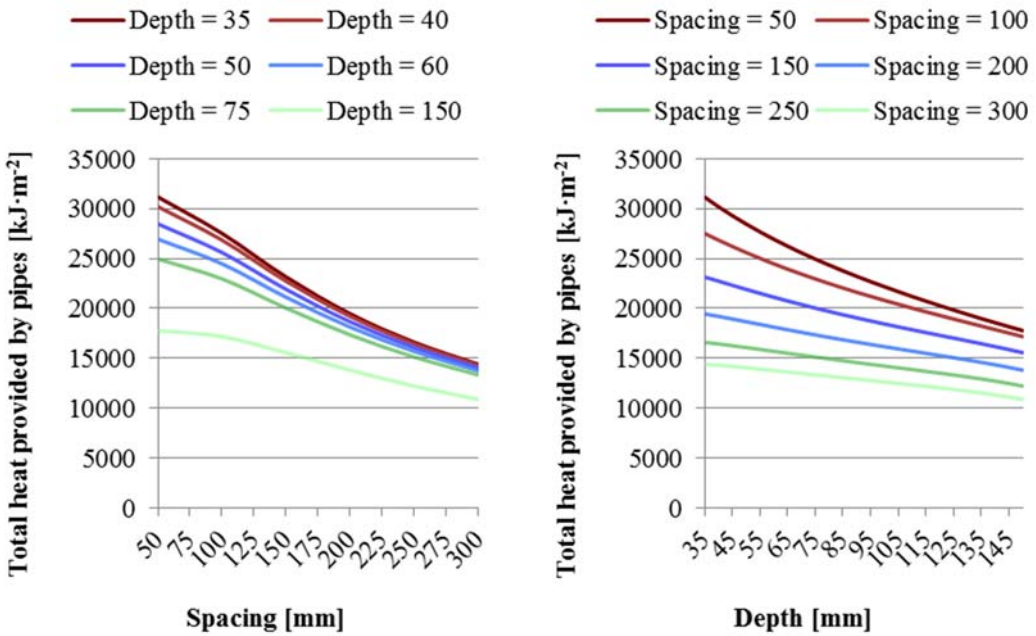

Figure 10. Influence of depth and spacing to heat supplied by the pipes

Finally, Figure 11 shows the ratio between the heat provided by the pipes and the heat transferred to indoor space, any result below one implies heat loses to outdoor ambiance. The results show that in any case most of the heat provided by the pipes was transferred to indoor space and heat losses to outdoor ambiance were very limited. The worst case was at maximum spacing and depth, in which the heat loses represented up to 15 % of the heat supplied. Furthermore, Figure 11 shows that heat loses increased proportionally as the depth increased. Additionally, the heat loses ratio increased fast at low spacing, while it stabilized about 125 mm.

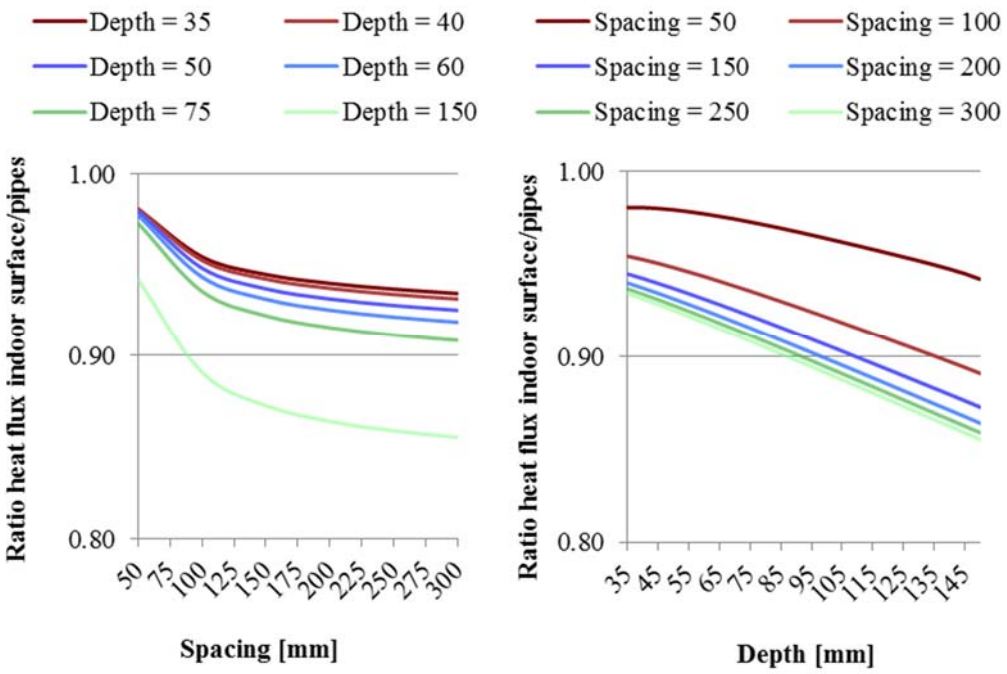

Figure 11. Ratio between heat flux through indoor surface and heat flux supplied by pipes

5.2 Influence of control strategy

The influence of the control strategy is presented in Figure 12, which shows that the total heat supplied by the pipes and the total heat exchanged on the indoor surface decreased as the activation periods were longer. As heat was supplied continuously during the activation periods, the temperature of the brick around the pipes increased, and thus the temperature gradient between the supply temperature and the brick decreased, reducing the heat transfer. Consequently, as the activation periods were shorter, the brick had time to homogenize its temperature and to release to heat to indoor ambient during off-periods, and then the temperature around the pipes decreased. In this case, the temperature gradient along each active period was maximized, and thus the overall heat transfer efficiency of the system was improved. As a result, in the studied case a control strategy with activation periods of 0.5 h delivered up to a 20 % more of heat than a 12 h strategy.

The difference in behaviour between 2 h activation strategy, 6 h activation strategy, and 12 h activation strategy is shown in Figure 13. Just before the activation the average temperature of the wall was lower for the longest activations strategies, as those had more time to cool between heating periods. Therefore, the heat transfer at the beginning of the 12 h strategy was better for the first hours. However, Figure 13 shows that after 6 h of heating the temperature of the wall with the 12 h strategy was the same that the temperatures at the end of the heating period of the

2 h strategy. Consequently, during most of the heating period of the 12 h strategy the temperatures of the wall were higher, and thus the heat transfer was worse due to lower temperature gradient.

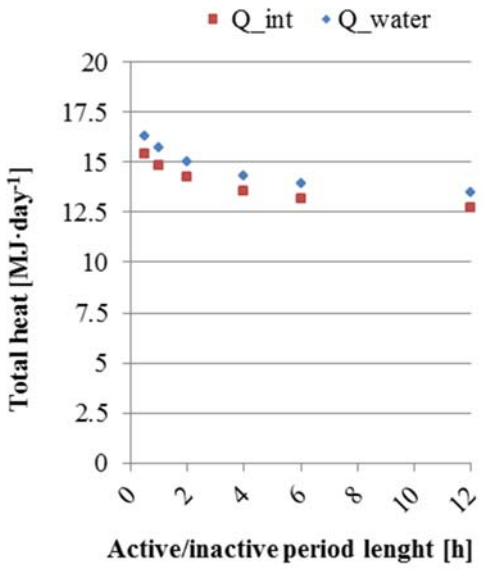

Figure 12. Total heat supplied by pipes depending on length of activation periods

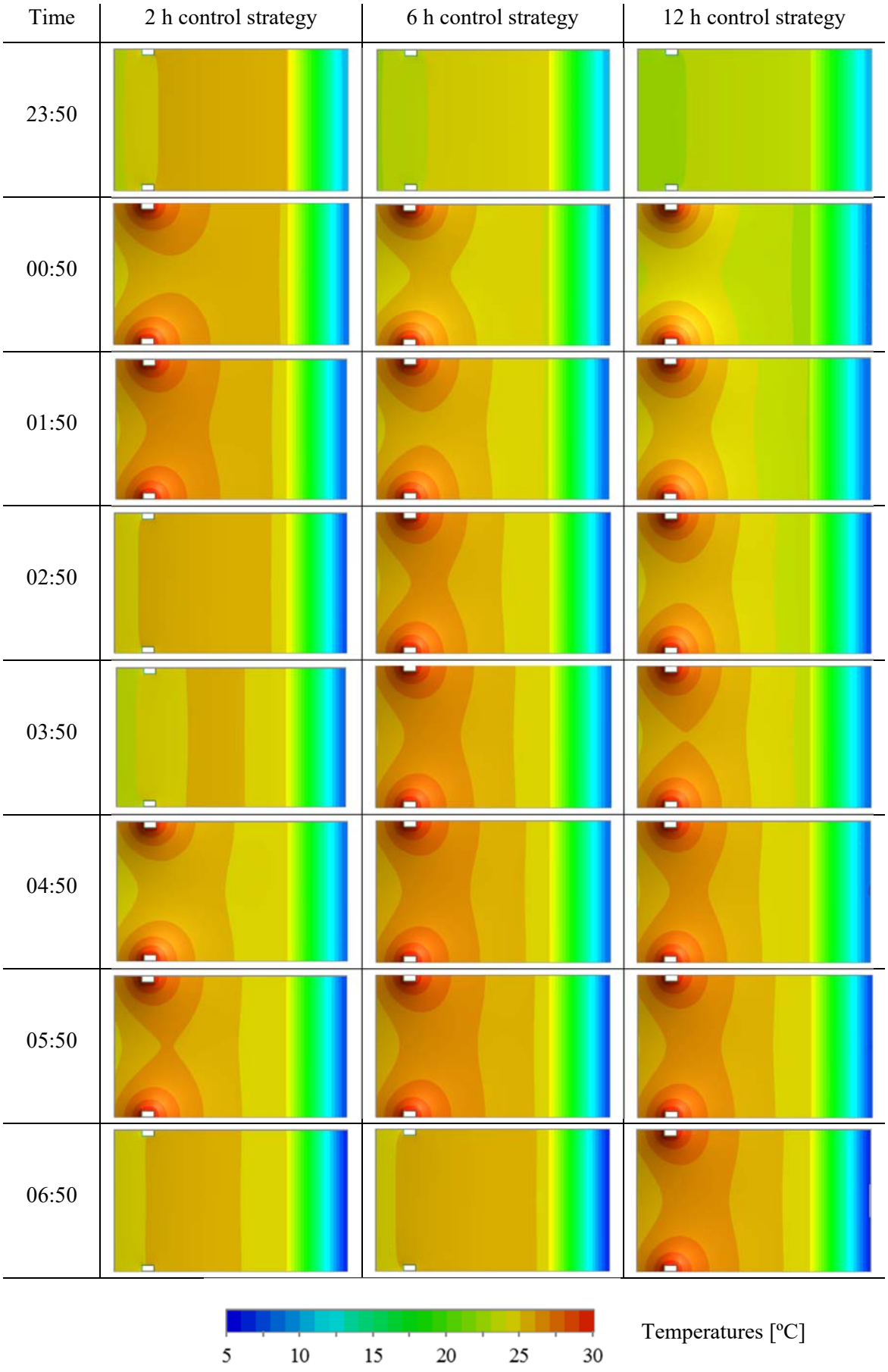

460 Figure 13. Radiant Wall temperature map evolution for control strategies 2 h, 6 h, and 12 h

The influence of the evolution of the temperature in the radiant wall is further explained in Figure 14. The heat flux provided by the pipes had a high transient peak at the beginning of each activation, but it later stabilized, which resulted in long activations periods achieving steady state. As the indoor air temperature, the water temperature, and the flow were considered constant, the system tended to stabilise at a heat flux dependant on the temperature gradient between the supply temperature and the indoor temperature. As shown in Figure 14 the heat flux stabilised at 300 W during the active periods of control strategies of 6 h and 12 h. In contrast, the 2 h strategy kept the heat flux provided by the pipes transient and above the steady state value, therefore, the 2 h strategy supplied more heat, as shown in Figure 15.

Finally, Figure 14 indirectly shows the influence of outdoor weather conditions to the radiant wall performance. The outdoor temperature in the simulation was always lower that the indoor temperature and the wall temperature, causing always heat loses to outdoor ambient. However, the solar radiation heated the outdoor surface of the wall, making it reach temperatures above 40 ºC. This reduced the heat loses and made the temperature of the wall increase, which is visible in the reduced heat flux from the pipes between 12.00 and 22:00 for control strategies of 2 h and 6 h in Figure 14. However, Figure 16 shows that the heat flux on the indoor surface of the wall also increased slightly for all strategies during daylight hours. The reduction of heat loses to the outdoor ambient increased the fraction of heat supplyed by the pipes being released to indoor space. Furthermore, the results suggest that the increase of the heat flux on the indoor surface had some lag compared to the peak of solar radiation.

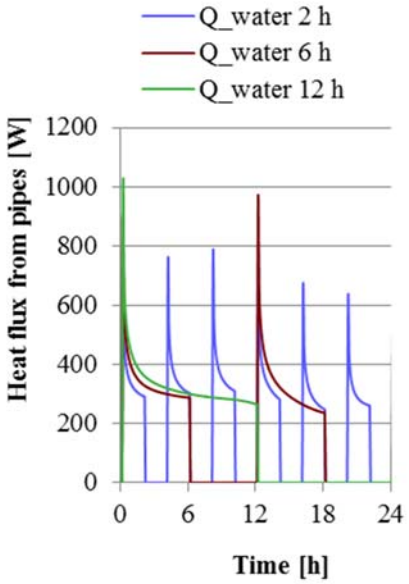

Figure 14. Heat flux on the pipes for control strategies of 2 h, 6 h, and 12 h

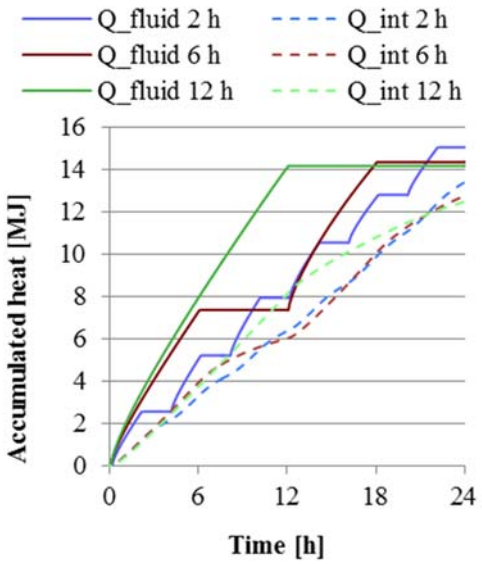

Figure 15. Total accumulated heat on the pipes and on the indoor surface for control strategies of 2 h, 6 h, and 12 h

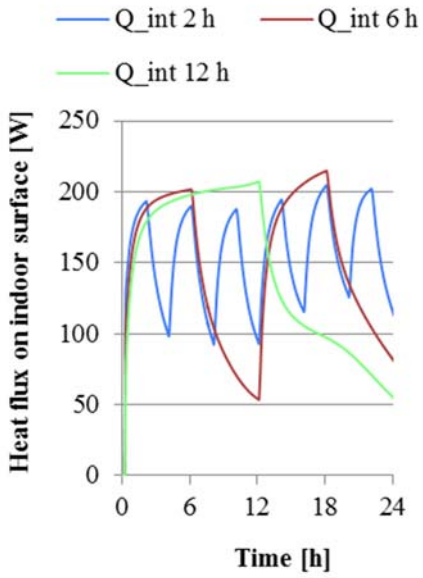

Figure 16. Heat flux on the indoor surface for control strategies of 2 h, 6 h, and 12 h

6 Discussion

The parametric study carried out with the validated model suggested that optimal pipes spacing would be between 125 mm and 150 mm while optimal depth would be between 45 mm and 65 mm, these values would maximise the heat flux and minimize the temperature difference on the indoor surface. The results obtained are coincident to the conclusions of previous studies in the

literature, despite the difference of design and operation conditions. First, few studies considered the TABS to be exposed to outdoor ambient. Moreover, most of the parametric studies found considered horizontal TABS such as ceiling slabs, in-floor slabs or radiant floors, both in heating and cooling mode. The difference in operation mode, cooling or heating, is especially relevant. The radiant wall was studied under heating conditions, in which the thermal mass was less relevant. In this conditions heat was continuously lost to outdoor ambient, therefore, insulation was more important regarding the system performance. In contrast in cooling season the heat flux changes direction along the day, and thus thermal mass helps delaying the heat waves. In a study on ceiling slabs in cooling mode Antonopoulos and Democritou [15] suggested that optimal spacing was between 100 mm and 300 mm. On a following study on the same system, Antonopoulos and Tzivandis [16] concluded that depth below 40 mm and spacing above 200 mm resulted in big temperature difference on the surface, which could cause discomfort. Similar results were reported by Babiak et al. [33], who specified that for low conductivity slabs the pipes should not be deeper than 75 to 100 mm. Additionally, maximum recommended thickness of the slabs was 200 mm.

However, the results contrast with the conclusions of Krzaczek and Kowalzuk [17], which suggest that the active layer had to be placed a near to outdoor insulation as possible, that was deeper inside the wall. The origin of this discrepancy was the purpose of the embedded pipes in each study. Krzaczek and Kowalzuk presented a thermal barrier, which objective was to reduce the heat losses from indoor space to outdoor. The embedded pipes kept the active layer of the wall at a higher temperature than it would have without it, consequently, the temperature gradient between the wall and the indoor space was lower, and thus the heat losses decreased. Therefore, the objective of the TB was not heating the indoor space, but to reduce the heating load. In contrast, the purpose of the radiant wall was active heating of the indoor space.

The results also suggest that the studied radiant wall was well insulated, as shown in Figure 11 the ratio between the total heat flux on the indoor surface was at least 85 % of the heat flux supplied. This is coincident with the results from Bojic et al. [34], which showed that increasing insulation in buildings with TABS reduced the heating load more than in buildings with radiators. This could be further complemented by results from Ma et al. [35], which concluded that TABS such as the radiant wall performed better in buildings with synergistically good thermal mass and thermal resistance.

On the control strategy side, the results agree with the conclusions of Olesen et al. [36], which suggested that shorter heating times improved the heat transfer. This concept was used in

advanced control strategies to reduce the pumping time and the energy use of the heating or cooling system [37,38]

Finally, the validation of this relatively simple mode was especially significant, as data was obtained from tests under outdoor conditions. Despite this added more assumptions in form of uncontrollable variables, the model achieved accurate results. Furthermore, the results were consistent with the literature.

7 Conclusions

A brickwork radiant wall was modelled and validated with a transient 2D finite volumes model. The model was validated with experimental data of a house-like cubicle, with simulations showing good agreement with the temperature profiles and the heat flux for walls with three different orientations. The comparison against the results from the literature reinforced the validity of the model for predicting the performance of the radiant wall and studying its design and control strategies.

The validation showed that assuming constant fluid temperature was reasonable, and therefore applying two dimensions and the consequent simplification from symmetry was acceptable. Furthermore, the correlations for convection and radiation heat transfer coefficients did not introduce significant errors. Consequently, the model was accurate and reliable for predicting the behaviour of a radiant wall exposed to outdoor ambiance.

The parametric study showed that spacing and depth strongly influence the behaviour of the radiant wall in terms of indoor surface temperature and heat flux. The obtained results pointed that spacing between 125 mm and 150 mm and depth between 45 mm and 65 mm maximized the heat flux and minimized the temperature difference on the indoor surface under the tested conditions.

Finally, shorter heating periods improved the efficiency of the radiant wall. During long activation the average temperature of the wall increased and thus the heat flux provided by the pipes decreased, as the temperature gradient between the supply water and the wall was lower.

The results showed the importance of simulation for improving the design of radiant wall as well as the control strategies. Furthermore, the reliability of the models needed to be validated with experimental data. The current research developed a model that can be further implemented on building models to study the interaction between the heating and cooling

systems and the dynamics of the building. Moreover, the simplifications derived from the assumptions resulted in a model with low computational effort, which could be useful for integration in full building models.

Acknowledgements

The work was partially funded by the Spanish government (ENE2015-64117-C5-1-R (MINECO/FEDER), ENE2015-64117-C5-3-R (MINECO/FEDER), and ULLE10-4E-1305). GREA is certified agent TECNIO in the category of technology developers from the Government of Catalonia. The authors would like to thank the Catalan Government for the quality accreditation given to their research group (2014 SGR 123) and the city hall of Puigverd de Lleida. This projects has received funding from the European Commission Seventh Framework Programme (FP/2007-2013) under Grant agreement Nº PIRSES-GA-2013-610692 (INNOSTORAGE) and from European Union's Horizon 2020 research and innovation programme under grant agreement Nº 657466 (INPATH-TES). Alvaro de Gracia would like to thank Ministerio de Economia y Competitividad de España for Grant Juan de la Cierva, FJCI-2014-19940.

590 **References**

591 1 Energy Technology Perspectives 2012, IEA, Paris, 2012

592 2 K.N. Rhee, K.W. Kim, A 50 year review of basic and applied research in radiant heating
593 and cooling systems for the built environment, Build. Environ., 91 (2015) 166-190

594 3 X. Xu, S. Wang, J. Wang, F. Xiao, Active pipe-embedded structures in buildings for
595 utilizing low-grade energy sources: A review, Energy Build., 42 (2010) 1567–1581

596 4 X. Xu, J. Yu, S. Wang, J. Wang, Research and application of active hollow core slabs in
597 building systems for utilizing low energy sources, Appl. Energy., 116 (2014) 424–435

598 5 J. Romaní, A. de Gracia, L.F. Cabeza, Simulation and control of thermally activated
599 building systems (TABS), Energy and Build., 127 (2016) 22-42

600 6 K.N. Rhee, B.W. Olesen, K.W. Kim, Ten questions about radiant heating and cooling
601 systems, Build. and Env. 112 (2017) 367-381

602 7 G.P. Henze, C. Felsmann, D.E. Kalz, S. Herkel, Primary energy and comfort performance
603 of ventilation assisted thermo-active building systems in continental climates, Energy
604 Build., 40 (2008) 99–111

605 8 B.W. Olesen, M. De Carli, M. Scarpa, M. Koschenz, Dynamic evaluation of the cooling
606 capacity of thermo-active building systems, ASHRAE Trans., 112 (1) (2006) 350–357

607 9 B. Lehmann, V. Dorer, M. Koschenz, Application range of thermally activated building
608 systems tabs, Energy Build., 39 (2007) 593–598

609 10 R.A. Meierhans, Room air conditioning by means of overnight cooling of the concrete
610 ceiling, ASHRAE Trans., 102 (1996) 693–697

611 11 J. Romaní, G. Pérez, A. de Gracia, Experimental evaluation of a cooling radiant wall
612 coupled to a ground heat exchanger, Energy and Build., 129 (2016) 484-490

613 12 J. Romaní, G. Pérez, A. de Gracia, Experimental evaluation of a heating radiant Wall
614 coupled to a ground source heat pump, Renew. Energy, 105 (2017) 520-529

615 13 J. Glembin, C. Büttner, J. Steinweg, G. Rockendorf, N.K Rudolph, J. Rust, Solar active
616 building with directly heated concrete floor slabs, Energy Procedia, 48 (2014) 561-570

14 R. Zmeureanu, P. Fazio, Thermal performance of a hollow core concrete floor system for passive cooling, Build. Environ., 23 (1988) 243–252

15 K.A. Antonopoulos, F. Democritou, Periodic steady-state heat transfer in cooling panels, Int. J. Heat Fluid Flow., 14 (1993) 94–100

16 K.A. Antonopoulos, C. Tzivanidis, Numerical solution of unsteady three-dimensional heat transfer during space cooling using ceiling-embedded piping, Energy, 22 (1997) 59–67

17 M. Krzaczek, Z. Kowalczuk, Thermal Barrier as a technique of indirect heating and cooling for residential buildings, Energy Build., 43 (2011) 823–837

18 X. Jin, X. Zhang X, Y. Luo, R. Cao, Numerical simulation of radiant floor cooling system: Effects of thermal resistance of pipe and water velocity on the performance, Build. Environ., 5 (2010) 2545-2552

19 M.S. Shin, K.N. Rhee, S.R. Ryu, M.S. Yeo, K.W. Kim, Design of radiant floor heating panel in view of floor surface temperatures, Build. and Environ., 92 (2015) 559-577

20 R. Holopainen, P. Tuomaala, J. Piippo, Uneven gridding of thermal nodal networks in floor heating simulations, Energy Build., 39 (2007) 1107–111

21 X. Xu, Q. Zhu, W. Jinbo, F. Xiao, Study of dynamic thermal performance of a active pipe-embedded building envelopes based on frequency-domain finite difference method, Trans. Electr. Electron. Circuits Syst. 3 (2013) 65-72

22 Q. Zhu, X. Xu, J. Wang, F. Xiao, Development of dynamic simplified thermal models of active pipe-embedded building envelops using genetic algorithm, Int. J. Therm. Sci. 76 (2014) 258-272

23 J. Xie, X. Xu, A. Li, Q. Zhu, Experimental validation of frequency-domain finite-difference model of active pipe-embedded building envelope in time domain by using Fourier series analysis, Energy and Build. 99 (2015) 177-188

24 Q. Zhu, A. Li, J. Xie, W. Li, X. Xu, Experimental validation of a semi-dynamic simplified model of active pipe-embedded building envelope, Int. J. Therm. Sci. 108 (2016) 70-80

25 C. Shen, X. Li, Dynamic thermal performance of pipe-embedded building envelope utilizing evaporative cooling water in the cooling season, App. Them. Eng. 106 (2016) 1103-1113

646 26 K.A. Antonopoulos, M. Vrachopoulos, C. Tzivandis, Experimental and theoretical studies
647 of space cooling using ceiling-embedded piping, Appl. Therm. Eng. 17 (1997) 351-367

648 27 O. Acikgoz, A. Çebi, A.S. Delkilic, A. Koca, G. Çetin, Z. Gemici, S. Wongwises, A novel
649 ANN-based approach to estimate heat transfer coefficients in radiant wall heating systems,
650 Energy and Build. 144 (2017) 401-415

651 28 Ecoforest, http://ecoforest.es (accessed Decembre 2016)

652 29 EN ISO 6946 (2007), Building components and building elements – Thermal resistance
653 and thermal transmittance – Calculation method

654 30 Y.A. Çengel, Heat transfer: A practical approach, McGrawHill (1998) International Edition

655 31 W.C. Swinbank, Q.J. Roy, Long-wave radiation from clear skies, Q. J. R. Meteorol. Soc.
656 89 (1936) 339

657 32 M. de Carli, M. Scarpa, R. Tomasi, A. Zarrella, DIGITHON: A numerical model for the
658 thermal balance of rooms equipped with radiant systems, Build. Environ., 57 (2012) 126-
659 144

660 33 J. Babiak, M. Minárová, B.W. Olesen, What is the effective thickness of a thermally
661 activated concrete slab, in: Proceedings of Clima, WellBeing Indoors, (2007)

662 34 M. Bojic, D. Cvetokovic, M. Miletic, J. Lamesevic, H. Boyer, Energy, cost, and CO2
663 emission comparison between radiant wall panels systems and radiator systems, Energy
664 Build. 54 (2012) 496-502

665 35 P. Ma, L.S. Wang, N. Guo, Modeling of TABS-based thermally manageable buildings in
666 Simulink, App. Energy, 104 (2013) 791-800

667 36 B.W Olesen, B. Lehman, J. Tödtli, V. Dorer, F. Renggli, Control of thermally-activated
668 building systems (TABS), Appl. Energy, 85 (2008) 565-581

669 37 S.H. Cho, M. Zaheer-Uddin, Predictive control of intermittently operated radiant floor
670 heating systems, Energy Convers. Manag., 44 (2003) 1333-1342

671 38 J. Feng, F. Chuang, F. Borreli, F. Bauman F, Model predictive control of radiant slab
672 systems with evaporative cooling sources, Energy Build. 87 (2014) 199-210
673
674